

Roles of Tyr¹²²-hydrophobic Cluster and K⁺ Binding in Ca²⁺-releasing Process of ADP-insensitive Phosphoenzyme of Sarcoplasmic Reticulum Ca²⁺-ATPase^{*[5]}

Received for publication, June 17, 2008, and in revised form, August 22, 2008. Published, JBC Papers in Press, August 26, 2008, DOI 10.1074/jbc.M804596200

Kazuo Yamasaki¹, Guoli Wang, Takashi Daiho, Stefania Danko, and Hiroshi Suzuki

From the Department of Biochemistry, Asahikawa Medical College, Asahikawa 078-8510, Japan

Tyr¹²²-hydrophobic cluster (Y122-HC) is an interaction network formed by the top part of the second transmembrane helix and the cytoplasmic actuator and phosphorylation domains of sarcoplasmic reticulum Ca²⁺-ATPase. We have previously found that Y122-HC plays critical roles in the processing of ADP-insensitive phosphoenzyme (E2P) after its formation by the isomerization from ADP-sensitive phosphoenzyme (E1PCa₂) (Wang, G., Yamasaki, K., Daiho, T., and Suzuki, H. (2005) *J. Biol. Chem.* 280, 26508–26516). Here, we further explored kinetic properties of the alanine-substitution mutants of Y122-HC to examine roles of Y122-HC for Ca²⁺ release process in E2P. In the steady state, the amount of E2P decreased so that of E1PCa₂ increased with increasing luminal Ca²⁺ concentration in the mutants with K_{0.5} 110–320 μM at pH 7.3. These luminal Ca²⁺ affinities in E2P agreed with those estimated from the forward and luminal Ca²⁺-induced reverse kinetics of the E1PCa₂-E2P isomerization. K_{0.5} of the wild type in the kinetics was estimated to be 1.5 mM. Thus, E2P of the mutants possesses significantly higher affinities for luminal Ca²⁺ than that of the wild type. The kinetics further indicated that the rates of luminal Ca²⁺ access and binding to the transport sites of E2P were substantially slowed by the mutations. Therefore, the proper formation of Y122-HC and resulting compactly organized structure are critical for both decreasing Ca²⁺ affinity and opening the luminal gate, thus for Ca²⁺ release from E2PCa₂. Interestingly, when K⁺ was omitted from the medium of the wild type, the properties of the wild type became similar to those of Y122-HC mutants. K⁺ binding likely functions via producing the compactly organized structure, in this sense, similarly to Y122-HC.

Sarcoplasmic reticulum Ca²⁺-ATPase (SERCA1a)² of the P-type ion-transporting ATPase family catalyzes Ca²⁺ trans-

port coupled with ATP hydrolysis from the cytoplasm to lumen against a concentration gradient of ~10,000-fold (1–8). In the initial steps (*steps 1 and 2* in Scheme 1), the enzyme is activated by binding of two cytoplasmic Ca²⁺ ions at the transport sites with a submicromolar high affinity (E2 to E1Ca₂). The activated enzyme is then auto-phosphorylated at Asp³⁵¹ by ATP and forms a phosphoenzyme intermediate (EP) (*step 3*), thereby the bound Ca²⁺ ions are occluded in the transport sites. This EP is rapidly dephosphorylated by ADP in the reverse reaction reproducing ATP, therefore “ADP-sensitive EP” (E1P). In the next step (*step 4*), E1PCa₂ is isomerized to the ADP-insensitive form, E2PCa₂. Upon this change at the catalytic site, the Ca²⁺ sites are deoccluded and opened to the luminal side, and the Ca²⁺ affinity is largely reduced, releasing the bound Ca²⁺ ions into the lumen (*step 5*). The Ca²⁺ release process is thought to be very rapid with the wild-type Ca²⁺-ATPase, and the accumulation of E2PCa₂ intermediate had actually never been found until we recently identified and trapped successfully this intermediate by a mutation study (9). In the final step, the Asp³⁵¹-acylphosphate of E2P is hydrolyzed to reproduce the dephosphorylated and inactive E2 form (*step 6*). The transport cycle is totally reversible, e.g. E2P can be formed from E2 by P_i in the absence of Ca²⁺, and the subsequent luminal Ca²⁺ binding to E2P produces E1PCa₂.

Three-dimensional structures in several intermediate states and their analogs have been solved (10–18). The Ca²⁺-ATPase has three cytoplasmic domains, P (phosphorylation), N (nucleotide binding), and A (actuator or anchor), and ten transmembrane helices (M1–M10). The two Ca²⁺ binding sites consist of residues on M4, M5, M6, and M8 (10). The P domain possesses the phosphorylation site (Asp³⁵¹) and is directly linked to the long helices M4 and M5. The ATP binding site is on the N domain connected to the P domain. The A domain is linked to M1, M2, and M3 via the A/M1-, A/M2-, and A/M3-linkers. The cytoplasmic three domains largely move and change their organization states during the Ca²⁺-transport cycle (19–21), and these changes are linked with the rearrangements in the transmembrane helices for the Ca²⁺ transport. As a most remarkable change, in the EP isomerization (loss of ADP sensitivity) and Ca²⁺ release, the A domain largely rotates and the P domain largely inclines toward the A domain, and these domains produce their tight association (see Fig. 1 for the change E1Ca₂·AlF₄⁻·ADP → E2·MgF₄²⁻ as the model for the overall process E1~PCa₂·ADP → E2·P_i, including the EP isomerization and Ca²⁺ release). These structural changes therefore involve distinct events in distinct regions, yet they

* This work was supported by a grant-in-aid for scientific research (C) (to K. Y.) and (B) (to H. S.) from the Ministry of Education, Culture, Sports, Science and Technology of Japan. The costs of publication of this article were defrayed in part by the payment of page charges. This article must therefore be hereby marked “advertisement” in accordance with 18 U.S.C. Section 1734 solely to indicate this fact.

[5] The on-line version of this article (available at <http://www.jbc.org>) contains supplemental Figs. S1–S6.

¹ To whom correspondence should be addressed: Dept. of Biochemistry, Asahikawa Medical College, Midorigaoka-Higashi, Asahikawa 078-8510, Japan. Tel.: 81-166-68-2353; Fax: 81-166-68-2359; E-mail: kyamasak@asahikawa-med.ac.jp.

² The abbreviations used are: SERCA1a, adult fast-twitch skeletal muscle sarcoplasmic reticulum Ca²⁺-ATPase; EP, phosphoenzyme; E1P, ADP-sensitive phosphoenzyme; E2P, ADP-insensitive phosphoenzyme; MOPS, 3-(N-morpholino)propanesulfonic acid; TG, thapsigargin; Y122-HC, Tyr¹²²-hydrophobic cluster.

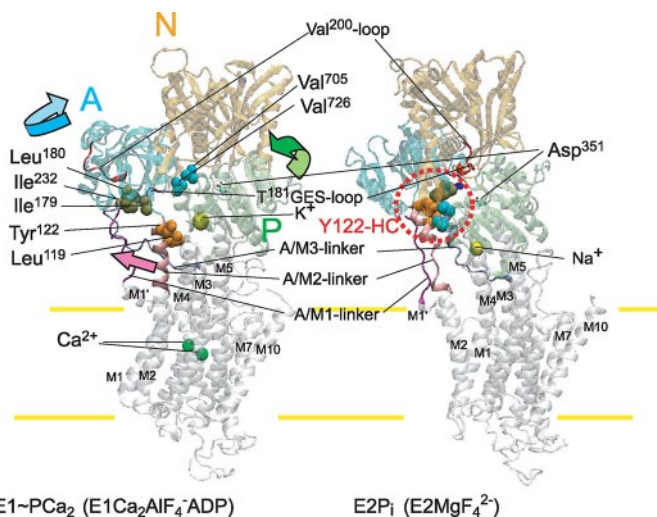
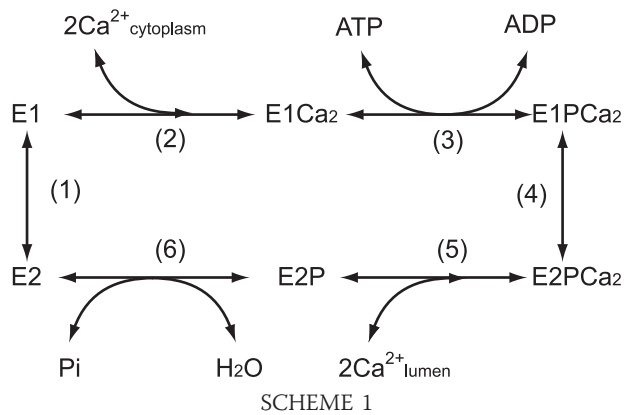


FIGURE 1. Structure of SERCA1a and formation of Tyr¹²²-hydrophobic cluster. The coordinates for the structures E1Ca₂·AlF₄⁻·ADP (the analog for the transition state of the phosphoryl transfer E1~PCa₂·ADP, left panel) and E2·MgF₄²⁻ (E2·P_i analog (21), right panel) of Ca²⁺-ATPase were obtained from the Protein Data Bank (PDB accession codes 1T5T and 1WPG, respectively (12, 14)). The arrows indicate approximate movements of the A and P domain and the top part of M2 (Leu¹¹⁹/Tyr¹²²) in the change from E1·AlF₄⁻·ADP to E2·MgF₄²⁻. The seven hydrophobic residues, Ile¹⁷⁹/Leu¹⁸⁰/Ile²³² on the A domain, Leu¹¹⁹/Tyr¹²² on the A/M2-linker, Val⁷⁰⁵/Val⁷²⁶ on the P domain are depicted as van der Waals spheres. They gather to form a hydrophobic cluster around Tyr¹²² in the change E1Ca₂·AlF₄⁻·ADP → E2·MgF₄²⁻ (Y122-HC, surrounded by the red dotted circle). The top part of M2, including Leu¹¹⁹/Tyr¹²², is unwound in E2·MgF₄²⁻, E2·AlF₄⁻, and E2·BeF₃⁻ with bound thapsigargin (TG), and thus becomes the A/M2-linker loop (see the region of M2 colored by pink).

are coordinated; namely 1) the loss of ADP sensitivity at the cytoplasmic region, 2) the decrease in the Ca²⁺ affinity at the transmembrane region, and 3) the opening of the Ca²⁺-releasing pathway (luminal gating).

Recently, we found that mutations in a specific hydrophobic interaction network, “Tyr¹²²-hydrophobic cluster” (Y122-HC), at the A-P domain interface disrupt markedly the processing of ADP-insensitive EP formed from ATP with Ca²⁺ and also the hydrolysis of E2P formed from P_i without Ca²⁺, thus causing nearly complete inhibition of the Ca²⁺-ATPase activity (22, 23). In these Y122-HC mutants, the high affinity binding of cytoplasmic Ca²⁺, the resulting E1PCa₂ formation, and the loss of the ADP sensitivity were all found to occur normally as in the wild type (22, 23). Y122-HC is formed by gathering of the seven residues of the three regions upon their motions; *i.e.* the largely

rotated A domain (Ile¹⁷⁹, Leu¹⁸⁰, and Ile²³²), the inclined P domain (Val⁷⁰⁵ and Val⁷²⁶), and the top part of the largely inclined M2 (or the A/M2-linker) (Leu¹¹⁹ and Tyr¹²²). Thus Y122-HC produces the compactly organized structure of E2P. Our previous analyses indicate that, in the Y122-HC mutants, there is a kinetic limit after the loss of ADP sensitivity and before the hydrolysis of the Ca²⁺-free E2P, therefore the Ca²⁺ release from E2PCa₂ is likely retarded (22, 23). Almost the same kinetic results were found with the mutations in another A-P domain interaction network at the Val²⁰⁰ loop of the A domain (24). Notably, E2PCa₂, the ADP-insensitive EP with two Ca²⁺ ions occluded at the transport sites was recently identified and trapped successfully by the elongation of the A/M1-linker with two or more amino acid insertions (9). In the elongation mutants, Y122-HC is not formed properly yet in E2PCa₂ trapped, but it is properly formed in the Ca²⁺-released form of E2P produced by P_i without Ca²⁺. Thus the observation is consistent with the involvement of Y122-HC in the Ca²⁺ release process from E2PCa₂.

In the present study, to further clarify roles of Y122-HC in the Ca²⁺ deocclusion/release processes and thus in the long range communication between the cytoplasmic and transmembrane regions, we explored kinetic features of the alanine-substitution mutants of Y122-HC. The results revealed that the mutations cause a marked increase in the apparent affinity of E2P for luminal Ca²⁺ and also a substantial retardation of the luminal Ca²⁺ access to E2P. Therefore, the formation of Y122-HC is critical for decreasing the affinity for Ca²⁺, for luminal gating (opening of the release pathway), and thus for Ca²⁺ release into lumen. Importantly, the assembling manner of the seven residues in Y122-HC in the very recently revealed crystal structure E2·BeF₃⁻ (17, 18) somewhat differs from that in E2·AlF₄⁻ and E2·MgF₄²⁻. Therefore, we discussed the significance of this difference in terms of the possible sequential gathering of the seven residues into Y122-HC on the basis of the observed difference in the extents of their mutational effects. In addition, we found with the wild type that its kinetic behavior became similar to that of Y122-HC mutants when K⁺ was omitted from the medium of the wild type. Results revealed for the first time the critical role of K⁺ binding in the wild type for Ca²⁺ deocclusion/release from E2PCa₂.

EXPERIMENTAL PROCEDURES

Mutagenesis and Expression—Mutations were created by the QuikChangeTM site-directed mutagenesis kit (Stratagene) and plasmid pGEM7-Zf(+) or pGEM3-Zf(+) (Promega, Madison, WI) containing ApaI-KpnI or KpnI-SalI fragments of rabbit SERCA1a cDNA as a template. The ApaI-KpnI or KpnI-SalI fragments were then excised from the products and used to replace the corresponding region in the full-length SERCA1a cDNA in the pMT2 expression vector (25). The pMT2 DNA was transfected into COS-1 cells by the liposome-mediated transfection method. Microsomes were prepared from the cells as described previously (26). The “control microsomes” were prepared from COS-1 cells transfected with the pMT2 vector containing no SERCA1a cDNA.

ATPase Activity—The rate of ATP hydrolysis was determined at 25 °C in a mixture containing 20 μg/ml microsomal

Tyr¹²²-hydrophobic Cluster of SERCA1a for Ca²⁺ Release

protein, 0.1 mM [γ -³²P]ATP, 3 μ M A23187, 0.1 M KCl, 7 mM MgCl₂, various concentrations of CaCl₂ up to 3 mM, 0.01 mM EGTA, and 50 mM MOPS/Tris (pH 7.3).

Formation and Hydrolysis of EP—Phosphorylation of SERCA1a in microsomes with [γ -³²P]ATP or ³²P_i and dephosphorylation of ³²P-labeled SERCA1a were performed under conditions described in the figure legends. The reactions were quenched with ice-cold trichloroacetic acid containing P_i. Rapid kinetics measurements of phosphorylation and dephosphorylation were performed with a handmade rapid mixing apparatus (27), otherwise the method was as above. The precipitated proteins were separated at pH 6.0 by 5% SDS-PAGE, according to Weber and Osborn (28). The radioactivity associated with the separated Ca²⁺-ATPase was quantitated by digital autoradiography as described previously (29). The amount of EP formed with the expressed SERCA1a was obtained by subtracting the background radioactivity with the control microsomes. This background was <1% of the radioactivity of EP formed with the expressed wild-type SERCA1a.

Miscellaneous—Protein concentrations were determined by the method of Lowry *et al.* (30) with bovine serum albumin as the standard. Free Ca²⁺ concentrations were calculated by the Calcon program. Data were analyzed by nonlinear regression using the program Origin (MicroCal Software, Inc., Northampton, MA). Three-dimensional models of the enzyme were reproduced by using the program VMD (31).

RESULTS

Ca²⁺-induced Change in Accumulation of ADP-insensitive EP in the Presence of 0.1 M K⁺ at Steady State—We first determined the steady state Ca²⁺-ATPase activity in the presence of increasing Ca²⁺ and ionophore A23187 with the alanine-substitution mutants of the seven residues of Y122-HC and the wild type. The Ca²⁺-ATPase activity was nearly completely inhibited in all the mutants in agreement with our previous observation (22, 23), and the complete inhibition was found at all the Ca²⁺ concentrations examined (see supplemental Fig. S1 for the representative mutant Y122A). Thus the possible luminal Ca²⁺ effect was not revealed by this type of measurements. Therefore in Fig. 2, to assess the affinity of the lumenally oriented Ca²⁺ transport site of E2P (known as the low affinity sites with the mM over ~10 mM K_d value), the amounts of ADP-insensitive EP were determined with the representative mutant Y122A at steady state at various Ca²⁺ concentrations and pH values in the presence of A23187 and KCl. The total amounts of EP (ADP-sensitive EP plus ADP-insensitive EP) were nearly the same under all the sets of conditions.

In the mutant Y122A, the fraction of the ADP-insensitive EP was very high at the low Ca²⁺ concentrations at all pHs (Fig. 2). This agrees with the property of this mutant (22, 23) that the hydrolysis of E2P is nearly completely inhibited thus causing its accumulation. The fraction of ADP-insensitive EP in the mutant markedly decreased, and it was converted to the ADP-sensitive EP with increasing Ca²⁺ concentration at several tens of micromolar to the sub-millimolar range. The apparent Ca²⁺ affinity in this Ca²⁺-induced change increased with increasing pH, and the Hill coefficients were found to be 2 in all pH values (see the legend to Fig. 2). In the wild type, the fraction of ADP-

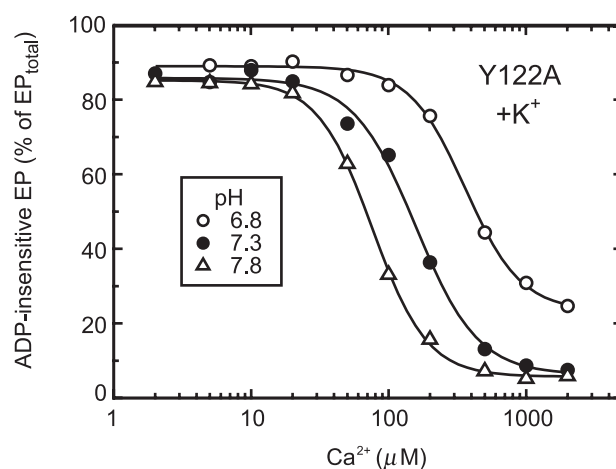


FIGURE 2. Ca²⁺ dependence of accumulation of ADP-insensitive EP in the steady state in mutant Y122A. Microsomes expressing the mutant Y122A were phosphorylated with [γ -³²P]ATP at various Ca²⁺ concentrations and pHs as indicated at 0 °C for 5 min in a mixture containing 20 μ g/ml microsomal protein, 50 mM MOPS/Tris, 0.1 M KCl, 7 mM MgCl₂, 0.01 mM EGTA, 3 μ M A23187, 10 μ M [γ -³²P]ATP, and various concentrations of CaCl₂. For the determination of the accumulated ADP-insensitive EP, an equal volume (50 μ l) of a mixture containing 10 mM ADP, 7 mM MgCl₂, 10 mM EGTA, 50 mM MOPS/Tris (pH 6.8, 7.3, or 7.8 as indicated), and 0.1 M KCl was added to the above phosphorylation mixture. At 1 s after this addition, the reaction was quenched with trichloroacetic acid. ADP-sensitive EP disappeared entirely within 1 s after the addition of ADP. The total amounts of EP were nearly the same under all the conditions (data not shown). The amount of ADP-insensitive EP is shown as a percentage of the total amount of EP. Solid lines show the least squares fit to the Hill equation. Apparent Ca²⁺ affinities and Hill coefficients thus obtained were 360 μ M and 2.1 (pH 6.8), 160 μ M and 1.9 (pH 7.3), and 76 μ M and 2.0 (pH 7.8).

insensitive EP was low at pH 7.3 and 7.8 being ~10% or less, and was a significant level, 35% at pH 6.8 (supplemental Fig. S2). These levels were not changed at 1 μ M to 3 mM Ca²⁺. Consistently, the luminal Ca²⁺ affinity of E2P of the wild type is known to be in the millimolar to 10 mM range (see Ref. 32–34). The results suggested that the luminal Ca²⁺ affinity of transport sites of E2P in the mutant may be significantly higher than that in the wild type.

Time Courses of Forward and Ca²⁺-induced Reverse Conversions between E1PCa₂ and E2P—In Fig. 3 with Y122A, the ADP-insensitive EP, and the ADP-sensitive EP was first accumulated at steady state at 10 μ M Ca²⁺ and 1 mM Ca²⁺, respectively, at pH 7.3. Then the Ca²⁺ concentration jump was made from 10 μ M to 1 mM or from 1 mM to 80 nM, and the change in the fraction of the ADP-insensitive EP was followed. Because the hydrolysis of E2P was nearly completely blocked in Y122A (with the rate \ll 0.01 s⁻¹) (22, 23), the time courses represent the forward and reverse isomerization between E1PCa₂ and E2P. When Ca²⁺ was increased from 10 μ M to 1 mM, the fraction of ADP-insensitive EP rapidly decreased from 80% to 10% (*i.e.* it was converted to the ADP-sensitive EP) with a rate 0.4 s⁻¹. On the other hand, when the Ca²⁺ concentration was decreased from 1 mM to 80 nM, *i.e.* virtually Ca²⁺ was removed, the ADP-sensitive EP was converted to the ADP-insensitive EP with a rate 0.022 s⁻¹.

Effect of Ca²⁺ Ionophore A23187 in Accumulation of ADP-insensitive EP—To ascertain that the Ca²⁺-dependent changes in the fraction of ADP-insensitive EP (Figs. 2 and 3) are caused by luminal Ca²⁺, we examined also in the absence of A23187

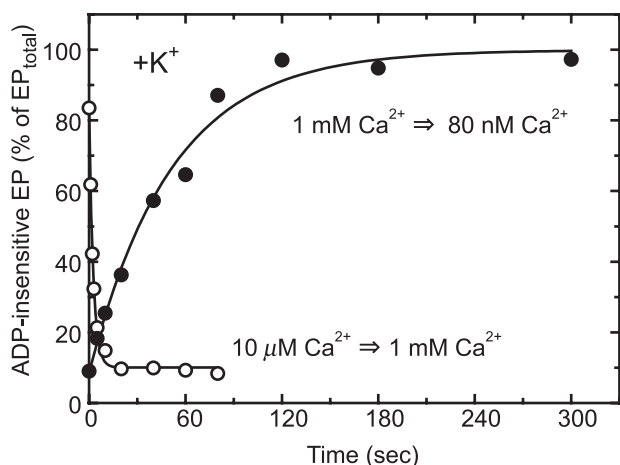


FIGURE 3. Time course of the change in the fraction of ADP-insensitive EP upon Ca²⁺-concentration jump. Microsomes expressing the mutant Y122A (20 μg/ml) were phosphorylated with [γ -³²P]ATP at pH 7.3 for 5 min in the presence of 10 μM (○) or 1 mM CaCl₂ (●) without EGTA in the phosphorylation solution otherwise as described in Fig. 2. Then an equal volume of the solution containing 2 mM CaCl₂ or 2 mM EGTA (otherwise as in the phosphorylation solution) was added to give final free Ca²⁺ concentrations 1 mM and 80 nM, respectively. At the indicated times after this Ca²⁺ jump, the total amount of EP and the amount of ADP-insensitive EP was determined as in Fig. 2. *Solid lines* show the least squares fit to a single exponential. The total amount of EP was not changed during the period of observation in both cases (data not shown). The amount of ADP-insensitive EP is shown as a percentage of the total amount of EP.

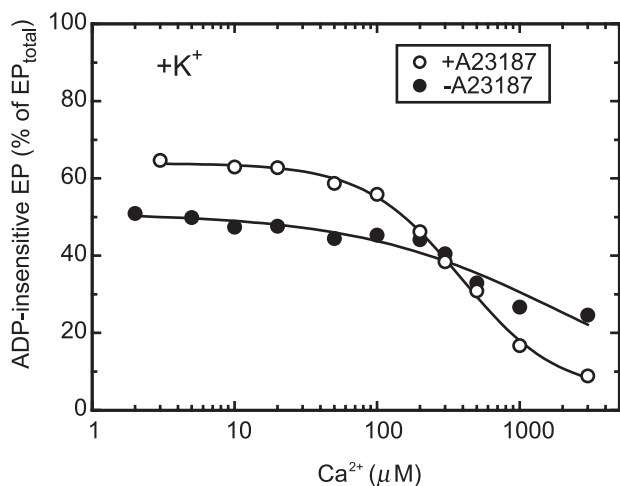


FIGURE 4. Effect of calcium ionophore on the Ca²⁺ dependence of ADP-insensitive EP accumulation in the steady state. Microsomes expressing the mutant Y122A (20 μg/ml) were phosphorylated at 0 °C for 5 min in the medium containing 50 mM MOPS/Tris (pH 7.3), 0.1 M KCl, 7 mM MgCl₂, 10 μM CaCl₂, 10 μM [γ -³²P]ATP, and 50 μM Ruthenium Red (to block Ca²⁺ channels as much as possible) in the presence (○) or absence (●) of 3 μM A23187. Then the free Ca²⁺ concentration was changed as indicated on the abscissa by mixing with an equal volume of a solution containing 50 mM MOPS/Tris (pH 7.3), 0.1 M KCl, 7 mM MgCl₂, 2 mM EGTA, and various concentrations of CaCl₂. After 10 s of this Ca²⁺ jump, the total amount of EP and the fraction of the ADP-insensitive EP were determined as described in Fig. 2. The inclusion of Ruthenium Red in the presence of A23187 caused a slight decrease in the ADP-insensitive EP fraction at the Ca²⁺ concentrations below ~100 μM (*cf.* Fig. 2) for unknown reasons.

the Ca²⁺ dependence of the steady-state fraction of ADP-insensitive EP (Fig. 4). The Ca²⁺-dependent change was rather small in the absence of A23187, in contrast to the very large change in its presence. Therefore, the observed Ca²⁺-induced conversion from the ADP-insensitive EP to ADP-sensitive one

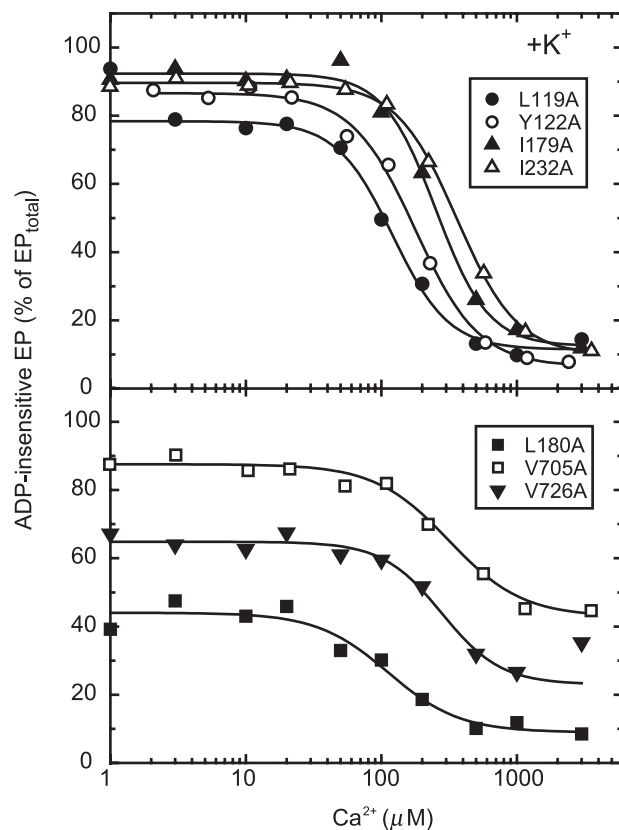


FIGURE 5. Ca²⁺ dependence of accumulation of ADP-insensitive EP in mutants for Tyr¹²²-hydrophobic cluster. Microsomes expressing each of the seven Y122-HC mutants (indicated in the figure) were phosphorylated with [γ -³²P]ATP at various concentrations of Ca²⁺ and pH 7.3, otherwise as described in Fig. 2. *Solid lines* show the least squares fit to the Hill equation. The fitting parameters, including the apparent Ca²⁺ affinity and the Hill coefficient, thus obtained are listed in Table 1.

in Y122A is due to the Ca²⁺ binding to the lumenally oriented transport sites.

Ca²⁺-induced Change in Accumulation of ADP-insensitive EP of Seven Y122-HC Mutants in the Presence of 0.1 M K⁺—In Fig. 5, each of the other six residues involved in the Y122-HC (Leu¹¹⁹/Ile¹⁷⁹/Leu¹⁸⁰/Ile²³²/Val⁷⁰⁵/Val⁷²⁶) was substituted with alanine, and its effect on the ADP-insensitive EP level was examined as in Fig. 2 in the presence of A23187 and K⁺. All the Y122-HC mutants exhibited the marked Ca²⁺-dependent change in the ADP-insensitive EP fraction.³ The apparent affinities for lumenal Ca²⁺ in the Y122-HC mutants were found to be between 110 and 320 μM with a Hill coefficient of ~2 (Table 1). The results showed that all these Y122-HC mutants possess the lumenally oriented transport sites with the affinities as high as that of Y122A.

Ca²⁺-induced Change in Accumulation of ADP-insensitive EP of Mutants and Wild Type in the Absence of K⁺—In Fig. 6, the same sets of steady-state analysis as in Fig. 2 were done with the wild type and Y122A but here in the absence of K⁺. It is well known (35, 36) that, in the absence of K⁺, the E2P hydrolysis of

³ The maximal level of the ADP-insensitive EP of L180A at low Ca²⁺ concentrations (44% of total amount of EP) was significantly lower than those of the other mutants. It may be due to the significantly faster E2P hydrolysis rate in L180A as compared with the rates in the others, as shown in supplemental Fig. S4.

Tyr¹²²-hydrophobic Cluster of SERCA1a for Ca²⁺ Release

TABLE 1

Parameters obtained for Ca²⁺ dependence of accumulation of ADP-insensitive EP in Y122-HC mutants

As shown in Fig. 5, the luminal Ca²⁺-induced change in the steady-state accumulation of ADP-insensitive EP of the seven Y122-HC mutants in the presence of 0.1 M K⁺ were fitted to the Hill equation. The parameters thus obtained by the least squares fit are listed here. K_{0.5} is the Ca²⁺ concentration giving the half-maximum change in the fraction of ADP-insensitive EP among the total amount of EP, therefore the apparent affinity for luminal Ca²⁺. The highest fraction of the ADP-insensitive EP at the low Ca²⁺ concentration range (0–10 μM) and its lowest fraction at the high Ca²⁺ concentration range (over ~mM) are also listed as the obtained parameters in the fitting (see Fig. 5). The value n_H is the Hill coefficient.

Mutant	Fraction of ADP-insensitive EP at highest and lowest Ca ²⁺ concentration ranges		K _{0.5}	n _H
	High Ca ²⁺	Low Ca ²⁺		
	% of total amount of EP			
L119A	11	78	0.12	2.1
Y122A	6	86	0.16	1.9
I179A	12	92	0.25	2.3
L180A	9	44	0.11	1.6
I232A	10	89	0.32	2.0
V705A	39	80	0.27	1.6
V726A	23	65	0.28	2.0

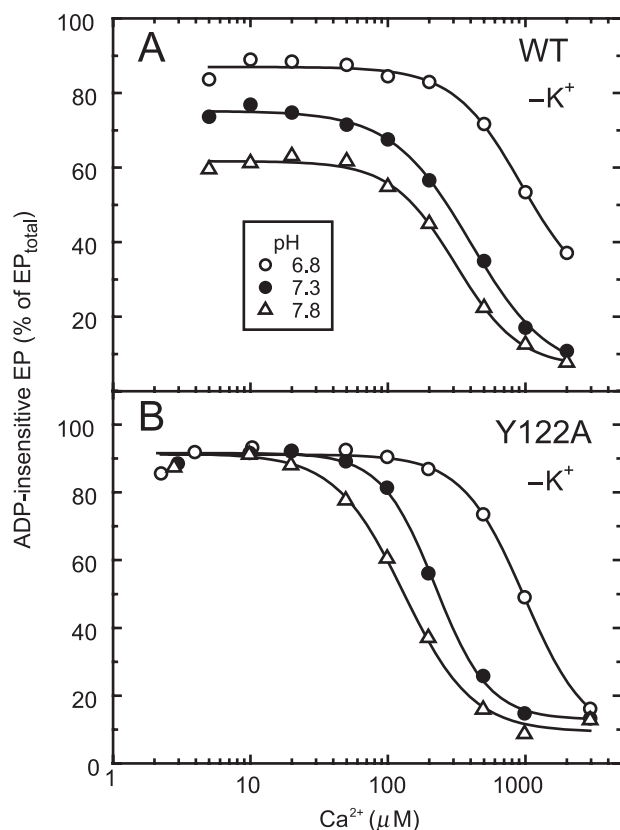


FIGURE 6. Ca²⁺ dependence of accumulation of ADP-insensitive EP in the absence of K⁺. Microsomes expressing the wild type (A) or Y122A (B) SERCA1a were phosphorylated with [³²P]ATP at various Ca²⁺ concentrations and pH (6.8 (○), 7.3 (●), and 7.8 (△)) in the presence of 0.1 M LiCl in place of KCl, otherwise under exactly the same conditions as those described in Fig. 2. The amount of ADP-insensitive EP was determined by addition of the ADP solution that contains 0.1 M LiCl in place of KCl otherwise as in Fig. 2. The total amount of EP was nearly constant under all the conditions (data not shown). The amount of ADP-insensitive EP is shown as a percentage of the total amount of EP. Solid lines show the least squares fit to the Hill equation. Apparent Ca²⁺ affinities and Hill coefficients thus obtained with the wild type (panel A) were 930 μM and 1.8 (pH 6.8), 400 μM and 1.5 (pH 7.3), and 310 μM and 1.9 (pH 7.8), and those obtained with Y122A (panel B) were 1000 μM and 1.9 (pH 6.8), 220 μM and 2.2 (pH 7.3), and 130 μM and 1.7 (pH 7.8).

the wild type is markedly slowed, and therefore the ADP-insensitive EP significantly accumulates. The fraction of ADP-insensitive EP in the wild type in the absence of K⁺ decreased with increasing Ca²⁺ concentration as in Y122A with the Hill coefficient ~2. The apparent affinity for luminal Ca²⁺ increased with increasing pH in the wild type as in Y122A. The pH-dependent changes are consistent with the fact that the residues for Ca²⁺ ligation at the transport sites are also involved in the proton binding (and its counter transport); the observed Ca²⁺-induced changes reflect the Ca²⁺ binding to the lumenally oriented transport sites of E2P. At each pH, the affinity of the wild type was similar to or slightly lower than that of Y122A. Thus in the absence of 0.1 M K⁺, the property of the wild type became similar to that of Y122A. In Y122A, elimination of K⁺ exhibited no significant effect on the apparent affinity for luminal Ca²⁺ (cf. Fig. 2).

The observed effect of K⁺ on the wild type is probably due to its binding in the cytoplasmic region. In crystallographic as well as mutational studies (12, 37), the K⁺ binding site of the Ca²⁺-ATPase was identified to be in the cytoplasmic region but not in the lumenal or transmembrane regions (see Fig. 11). Actually, we found experimentally that, when K⁺ at 0.1 M was added without any K⁺-ionophore to the Ca²⁺-ATPase in SR vesicles phosphorylated in the absence of K⁺, the Ca²⁺-dependence of the ADP-insensitive EP fraction observed as in Fig. 6A became immediately (within 10 s after the K⁺ addition) that in the presence of 0.1 M K⁺ as in supplemental Fig. S2 (data not shown).

Kinetics of Luminal Ca²⁺-induced E2P to E1PCa₂ Reverse Transition Followed by Its ADP-induced Rapid Decay to E1Ca₂ in the Presence of 0.1 M K⁺—Then with the representative mutant Y122A, we explored kinetically the luminal Ca²⁺ accessibility to the lumenally oriented transport sites of E2P formed from P_i without Ca²⁺ and the resulting luminal Ca²⁺-induced E2P to E1PCa₂ reverse transition. In Fig. 7, we included ADP and thereby followed the Ca²⁺- and ADP-induced decay of E2P to E1Ca₂ via E1PCa₂ in the reverse reaction. The E2P hydrolysis in the absence of Ca²⁺ was extremely slow (as previously demonstrated with the Y122-HC mutants (22, 23)), and the E2P decay was dramatically accelerated by the addition of Ca²⁺ and ADP (Fig. 7A). For example, the rate in the presence of 1 mM Ca²⁺ was 200-times faster than that of the forward E2P hydrolysis in the absence of Ca²⁺. ADP alone without Ca²⁺ or Ca²⁺ alone without ADP did not accelerate the EP decay (data not shown). As shown in Fig. 3, the increase of Ca²⁺ to 1 mM converted the ADP-insensitive EP (E2P) to the ADP-sensitive one (E1PCa₂), and E1PCa₂ thus formed was not decomposed in the absence of ADP. Therefore the Ca²⁺- and ADP-induced decay of E2P in Fig. 7A obviously occurred in the reverse reaction by the luminal Ca²⁺ binding; E2P + 2Ca²⁺ → E1PCa₂, then E1PCa₂ + ADP → E1Ca₂ + ATP (Scheme 1). This view agrees with the previous demonstration with SR Ca²⁺-ATPase (34). The rate of the EP decay in the presence of Ca²⁺ and ADP increased almost linearly with increasing Ca²⁺ concentrations and was not saturated even at 3 mM (Fig. 7B).⁴ Here, note that

⁴ Its slope was approximately 0.2 s⁻¹mM⁻¹ at 0–2 mM Ca²⁺. In Fig. 3, the rate of the forward E1PCa₂ to E2P conversion was estimated to be 0.02 s⁻¹. Therefore the calculation with these values, 0.02 s⁻¹ divided by

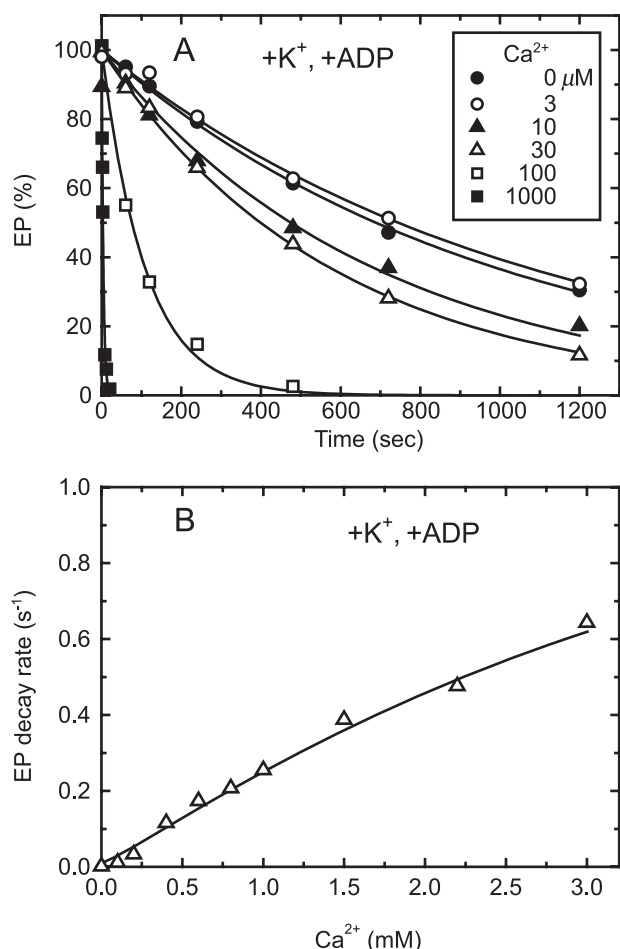


FIGURE 7. Lumenal Ca²⁺- and ADP-induced reverse E2P decay of Y122A in the presence of K⁺. A, microsomes (100 μg/ml) expressing the mutant Y122A were phosphorylated with ³²P_i for 10 min at room temperature in the absence of Ca²⁺ in a medium containing 50 mM MOPS/Tris (pH 7.3), 7 mM MgCl₂, 1 mM EGTA, 15 μM A23187, 0.1 mM ³²P_i, and 20% Me₂SO (that favors extremely the E2P formation (38)), and then the reaction mixture was chilled on ice. Subsequently, the phosphorylated sample was diluted at 0 °C with a 20-fold volume of a chase solution containing 50 mM MOPS/Tris (pH 7.3), 105 mM KCl, 7 mM MgCl₂, 1 mM EGTA, 0.1 mM non-radioactive P_i, and 0.105 mM ADP without or with various concentrations of CaCl₂ to give the final free Ca²⁺ concentrations as indicated. At the indicated periods, the chase reaction was terminated by trichloroacetic acid and the amount of EP was determined. Solid lines show the least squares fit to a single exponential decay. The decay rates thus obtained were plotted versus the Ca²⁺ concentration in panel B.

the steady-state level of ADP-sensitive EP (E1PCa₂) in the conversion from the ADP-insensitive EP (E2P) upon the lumenal Ca²⁺ binding in Y122A was almost fully saturated at 1 mM Ca²⁺ (see Fig. 2 at pH 7.3). The results indicate that the lumenal Ca²⁺ binding to E2P and formation of E2PCa₂ (E2P + 2Ca²⁺ → E2PCa₂) is likely the rate-limiting for the overall Ca²⁺- and ADP-induced reverse decay via the E2P to E1PCa₂ conversion with subsequent extremely rapid ADP-induced E1PCa₂ decay to E1Ca₂. This means that the slope in Fig. 7B of the Ca²⁺ dependence probably reflects the rate constant for the lumenal Ca²⁺ access and binding to the lumenally oriented transport sites of E2P and resulting E2PCa₂ formation.

0.2 s⁻¹ mM⁻¹, gave the apparent affinity for lumenal Ca²⁺ in E2P of Y122A as 100 μM. This value agreed very well with that (160 μM) obtained in Fig. 2 under the same conditions (pH 7.3) at the steady state.

The Ca²⁺- and ADP-dependent acceleration of the reverse E2P decay was assayed also with all the other Y122-HC mutants (supplemental Fig. S3). The rates of the reverse E2P decay increased almost linearly with increasing Ca²⁺ concentrations even at 3 mM, except those of I232A and V705A⁵ over ~1 mM Ca²⁺. Nevertheless, the slope of the Ca²⁺ dependence below 1 mM Ca²⁺ was estimated to be ~0.2 s⁻¹ mM⁻¹ in all the mutants as in Y122A. Therefore, the rate of the lumenal Ca²⁺ access and binding to the transport sites is similar in all the mutants of Y122-HC.

Kinetics of Lumenal Ca²⁺ Access to E2P of Wild Type and Y122A with and without K⁺—Then in Fig. 8, with the wild type and the representative mutant Y122A in the presence and absence of 0.1 M K⁺, we analyzed the Ca²⁺- and ADP-dependent acceleration of the reverse decay of E2P formed from P_i without Ca²⁺. As the well characterized property of the wild type, the forward hydrolysis of E2P without bound Ca²⁺ is very slow in the absence of K⁺, but markedly accelerated and thus very rapid in the presence of 0.1 M K⁺ (35, 36) (see the rates without Ca²⁺ in Fig. 8A). Nevertheless, even with the wild type in the presence of K⁺, we observed an apparently single exponential decay of E2P after the addition of Ca²⁺ and ADP at all the Ca²⁺ concentrations examined (time courses are not shown for simplicity). This is consistent with the kinetics described in the textbook by Fersht (39) that, in the parallel reactions in which a compound undergoes two or more single-step reactions simultaneously, its disappearance rate is described by a single exponential decay. In our case, the two reactions are the forward E2P hydrolysis and the Ca²⁺-/ADP-induced reverse E2P decay. The single decay rates thus obtained are plotted in Fig. 8A.

In the wild type in the presence of 0.1 M K⁺, the Ca²⁺ dependence of the EP decay rate was complicated because of the rapid E2P hydrolysis without Ca²⁺ (~0.4 s⁻¹), no change in the rate at 0–0.6 mM Ca²⁺, and the gradual increase above 0.6 mM. On the other hand, in the wild type in the absence of K⁺ in which the E2P hydrolysis without bound Ca²⁺ is markedly slowed, the nearly linear increase in the rate of Ca²⁺-/ADP-induced reverse E2P decay was observed at least up to ~3 mM Ca²⁺ as in the Y122-HC mutants in the presence of K⁺. The slope of the wild type without K⁺ was actually close to that of Y122A with K⁺. Therefore, the rate of lumenal Ca²⁺ access and binding to the transport sites of E2P of the wild type in the absence of K⁺ is similar to that of Y122A. With the wild type in the presence of K⁺, evaluation of the lumenal Ca²⁺ access rate by this approach was not possible because of the complicated Ca²⁺-dependence curve. In Y122A, little effect was seen when K⁺ was omitted at 0–1 mM Ca²⁺, although the slope became gradually less steep at the higher Ca²⁺ concentration in the absence of K⁺.

In Fig. 8B, by using the rates of the E2P decay in the presence of added Ca²⁺ and ADP (determined in Fig. 8A) and the rates of

⁵ As a possible reason for the less steep Ca²⁺-dependent curve observed with I232A and V705A over ~1 mM, it might be possible that the rate in the transition from E2PCa₂ to E1PCa₂ is slower in these mutants than in the other mutants, and this step became rate-limiting at the high Ca²⁺ concentrations where the lumenal Ca²⁺-induced change to E2PCa₂ became fast.

Tyr¹²²-hydrophobic Cluster of SERCA1a for Ca²⁺ Release

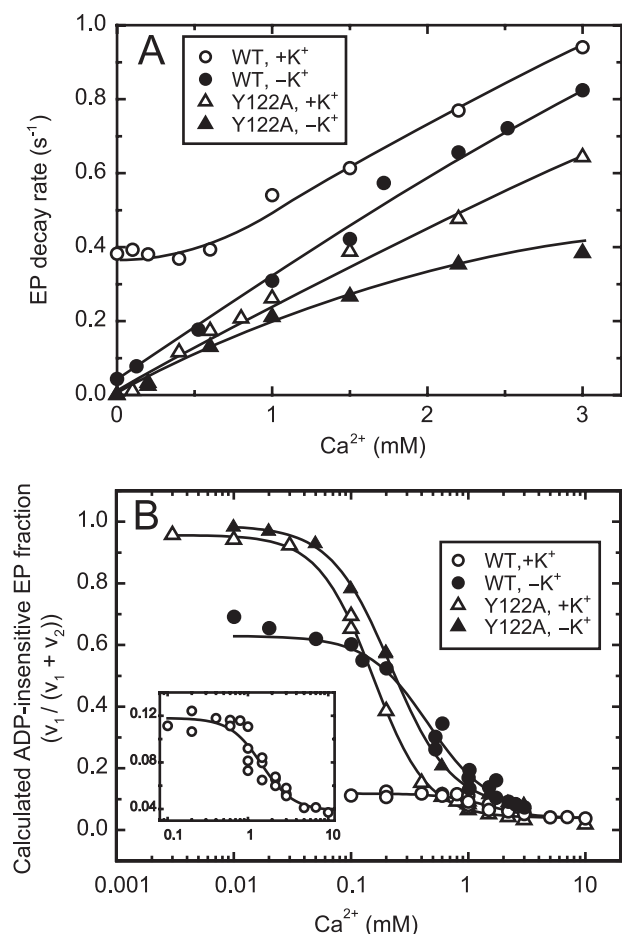


FIGURE 8. Luminal Ca²⁺- and ADP-induced reverse E2P decay of wild type and Y122A in the absence and presence of K⁺. *A*, microsomes (100 $\mu\text{g}/\text{ml}$) expressing wild type (WT) or Y122A were phosphorylated with ³²P_i in the presence of A23187 and absence of Ca²⁺, and then chilled on ice, as described in Fig. 7. Subsequently, the phosphorylated sample was diluted at 0 °C with a 20-fold volume of a chase solution containing non-radioactive P_i, various concentrations of CaCl₂, and ADP in the presence of 105 mM KCl (*open symbols*) or 105 mM LiCl in place of KCl (*closed symbols*), otherwise as described in Fig. 7. The time courses of EP decay were fitted to single exponential (data not shown, see Fig. 7A as an example). The rates thus obtained were plotted versus the Ca²⁺ concentrations. *B*, the fraction ADP-insensitive EP (F_{E2P}) in the total amount of EP at steady state was simulated by using the rate of E2P decay (v_2) and the rate of the E1PCa₂ to E2P isomerization (loss of ADP sensitivity, v_1) with an equation $F_{E2P} = v_1/(v_1 + v_2)$. Here, v_2 is the E2P decay rate obtained above in *panel A* at each Ca²⁺ concentrations. The v_1 was obtained as described in Fig. 3 by the Ca²⁺ jump experiments from high (1 mM) to low (80 nM, virtually Ca²⁺ removal) for Y122A with 0.1 M K⁺ or Li⁺ (without K⁺) and for the wild type with 0.1 M Li⁺ (without K⁺). For the wild type with 0.1 M K⁺, the forward decay rate of E1PCa₂ formed from ATP was used as the v_1 value, because the E1PCa₂ to E2P transition (the loss of ADP sensitivity) is rate-limiting for the E1PCa₂ decay via E2P and its subsequent rapid hydrolysis. The v_1 values actually used for the calculation were 0.049 s⁻¹ (wild type with K⁺), 0.071 s⁻¹ (wild type with Li⁺), 0.021 s⁻¹ (Y122A with K⁺), and 0.034 s⁻¹ (Y122A with Li⁺). The fraction of ADP-insensitive EP thus calculated was plotted versus the Ca²⁺ concentrations. The *solid lines* show the least squares fit to the Hill equation. In the *inset*, the ordinate is in a magnified scale for wild type with K⁺. In Table 2, the affinities and the Hill coefficients of the wild type and the Y122-HC mutants thus “estimated by kinetic analyses” in the absence and presence of K⁺ at pH 7.3 are summarized together with those actually “determined by the steady-state analyses” of the luminal Ca²⁺-induced change of the fraction of ADP-insensitive EP otherwise under the same conditions in Figs. 2 and 6.

the forward E1PCa₂ to E2P transition (as determined in Fig. 3), we simulated the fraction of the steady-state level of the ADP-insensitive EP (E2P) in the total amount of EP at each Ca²⁺ concentration. Note that this simulation was made possible by

TABLE 2
Affinities of E2P for luminal Ca²⁺ estimated by kinetic analyses and those determined at steady-state analyses

As described in Fig. 8B, the luminal Ca²⁺ affinities ($K_{0.5}$) of E2P of the wild type and the mutant Y122A were estimated by the kinetic analyses of the luminal Ca²⁺-induced E2P to E1PCa₂ reverse transition and of the forward E1PCa₂ to E2P transition. The $K_{0.5}$ values and the Hill coefficients (n_H) thus estimated kinetically in Fig. 8 in the absence and presence of 0.1 M K⁺ at pH 7.3 are summarized here. Listed together are those determined by the steady-state analyses of the luminal Ca²⁺-induced change in the accumulated fraction of the ADP-insensitive EP (E2P) under otherwise the same conditions in Figs. 2 and 6 for the mutant Y122A with and without K⁺ and the wild type without K⁺.

	K ⁺ (0.1 M)	Estimated by kinetic analyses		Determined by steady-state analyses	
		$K_{0.5}$	n_H	$K_{0.5}$	n_H
		<i>mM</i>		<i>mM</i>	
WT	+	1.48	2.2	— ^a	— ^a
	–	0.45	1.7	0.40	1.5
Y122A	+	0.15	1.9	0.16	1.9
	–	0.22	1.7	0.22	2.2

^a Not determined because the accumulation of ADP-insensitive EP was very low at all the Ca²⁺ concentrations examined, and therefore possible change was not revealed.

the fact that nearly all the phosphorylation sites are phosphorylated at steady state (in either E1P or E2P form) under the conditions used for the steady-state and kinetic analyses at all the Ca²⁺ concentrations in this study. Namely, the E2 to E1Ca₂ transition and the E1PCa₂ formation from E1Ca₂ with ATP are rapid enough to be ignored from the simulation. Therefore, the fraction of ADP-insensitive EP (E2P) in the steady state will be determined by the rate of its formation in the forward E1PCa₂ to E2P transition, v_1 , and by the rate of its decay, v_2 that includes both the forward hydrolysis of Ca²⁺-unbound E2P to E2 and the Ca²⁺-induced reverse transition to E1PCa₂ with the subsequent ADP-induced decay. This means that the simulation can be made even with the wild type in the presence of K⁺ (as v_2 can include the forward E2P hydrolysis). In the steady-state conditions, the decay rate (v_2) and formation rate (v_1) should be equal, therefore the fraction of ADP-insensitive EP (F_{E2P}) in the total amount of EP will be estimated by an equation: $F_{E2P} = v_1/(v_1 + v_2)$. Here, the E2P decay rate (v_2) was obtained in Fig. 8A at each Ca²⁺ concentration. The E1PCa₂ to E2P transition rate (v_1) was estimated from the Ca²⁺ jump experiments from high (1 mM) to low (80 nM) for Y122A with and without 0.1 M K⁺ and the wild type without K⁺, as described in Fig. 3. With the wild type in the presence of 0.1 M K⁺, the forward decay rate of E1PCa₂ formed by ATP was used as v_1 , because the E1PCa₂ to E2P transition (the loss of ADP sensitivity) is rate-limiting for the E1PCa₂ decay via E2P and its hydrolysis.

The Ca²⁺-dependent curves thus obtained by the simulation for the steady-state level of ADP-insensitive EP for Y122A with and without K⁺ and the wild type without K⁺ agreed very well with the respective ones determined at the steady state (*cf.* Figs. 2 (with K⁺) and 6 (without K⁺) at pH 7.3). The affinities for luminal Ca²⁺ estimated from the simulated curves are in fact almost the same as those actually determined at steady state (Table 2). The agreements assure the validity of the simulation and further allow us to estimate the luminal Ca²⁺ affinity of E2P of the wild type in the presence of K⁺. In the simulation for the wild type in the presence of K⁺ (*open circles* and *inset* in Fig. 8B), the fraction of ADP-insensitive EP was very low, and the extent of its change was extremely small as expected from the

steady-state measurements (*cf.* supplemental Fig. S2 (pH 7.3)). The apparent affinity of wild type for luminal Ca²⁺ in the presence of K⁺ was thus estimated by the small change to be 1.5 mM (see Table 2). This affinity was ~3.5-times lower than that of wild type without K⁺ and 10-times lower than that of Y122A with and without K⁺. Thus, by omitting K⁺, the luminal Ca²⁺ affinity of E2P in the wild type became higher and similar to that in Y122A.

Kinetics of Luminal Ca²⁺-induced E2P to E1PCa₂ Reverse Transition of E2P of Wild Type in the Presence of 0.1 M K⁺ Was Revealed by the Absence of ADP—Unfortunately, in the above experimental design and approach of Fig. 8A, we were not able to estimate the luminal Ca²⁺ access rate in E2P of the wild type in the presence of K⁺ because of the observed complexity of the Ca²⁺-dependent curve. In Fig. 9, we therefore employed a modified and thus different approach to examine the luminal Ca²⁺-induced reverse conversion from E2P to E1PCa₂. Namely, E2P was formed with P_i, and then a medium containing various concentrations of Ca²⁺ but without ADP (in contrast to its presence in Fig. 8) was added to E2P, and the subsequent EP decay was followed (Fig. 9A). In the absence of Ca²⁺, E2P was all hydrolyzed rapidly to E2 in a single exponential function. The E2P hydrolysis was inhibited gradually with increasing Ca²⁺ concentrations (over 0.1 mM), and the decay time course became biphasic as typically seen with 1 mM Ca²⁺. With increasing Ca²⁺ concentration, the fraction of the first and rapid phase decreased, that of the second phase increased, and the rate of the second phase became slower. The observation agrees with the previous kinetics analysis (9, 40). The first phase corresponds to the rapid and forward hydrolysis of the Ca²⁺-unbound E2P to E2. The EP species in the second phase was all ADP-sensitive (data not shown), therefore E1PCa₂ formed from E2P by the luminal Ca²⁺ binding. E1PCa₂ decayed very slowly in the absence of ADP, because the E1PCa₂ to E2P transition is much slower than the E2P hydrolysis, and this transition is retarded by the Ca²⁺ replacement of Mg²⁺ at the catalytic site of E1PCa₂ at the approximately millimolar high Ca²⁺ concentrations (41, 42).

The fraction of the second and slow phase of the EP decay was obtained by extrapolating to the zero time and plotted *versus* the Ca²⁺ concentration (Fig. 9B). The plot showed saturation at 5–10 mM Ca²⁺. Here it is critical to note that, as previously discussed in detail (9), the fraction of EP of the second phase (the fraction remaining after the first phase) is dependent on the ratio between the rates of the forward E2P hydrolysis and of the reverse E2P to E1PCa₂ conversion upon the luminal Ca²⁺ binding to E2P. Namely, the plot in Fig. 9B reflects the relation between these forward and reverse rates of E2P rather than the luminal Ca²⁺ affinity of E2P. For example, at the 50% saturation of the curve, the rate of the Ca²⁺-induced E1PCa₂ formation from E2P is equal to that of the E2P hydrolysis to E2. Then in Fig. 9C for the wild type in the presence of K⁺, the rate of the E1PCa₂ formation from E2P by the luminal Ca²⁺ binding to E2P was calculated (k_{rev} , open circles) at each Ca²⁺ concentration by using the fraction of the slow and second phase (F_s) and the E2P hydrolysis rate (k_h) with the equation, $k_{\text{rev}} = k_h F_s / (1 - F_s)$. The rate increased largely with increasing Ca²⁺ concentration.

In this kinetics, we eliminated the contribution of forward E2P hydrolysis on the overall E2P decay kinetics, and thereby revealed the rate of reverse E2P transition to E1PCa₂ induced by the luminal Ca²⁺ binding of the wild type in the presence of K⁺. For comparison in Fig. 9C, the rates of the luminal Ca²⁺-induced reverse E2P decay estimated for the wild type without K⁺ and Y122A with K⁺ in Fig. 8A were replotted. Note again that, in these cases, the hydrolysis of Ca²⁺-unbound E2P was very slow and retarded; therefore, the observed Ca²⁺-ADP-induced decay rates in their linear regions up to 3 mM Ca²⁺ reflect mostly the rates of the luminal Ca²⁺ access and binding to E2P in the reverse E2P decay. Note also that the experimental design in Fig. 9A employed for the wild type with K⁺ was not applicable to the wild type without K⁺ and Y122A, because the E2P hydrolysis is very slow and almost completely retarded in these cases, and therefore the E2P decay upon the Ca²⁺ addition cannot be described as the biphasic decay. Conversely, the experimental design employed in Fig. 8A to estimate the rates of the luminal Ca²⁺ access was not applicable to the wild type in the presence of K⁺ because of the complexity of the Ca²⁺-dependent curve as described above in Fig. 8A.

Thus in Fig. 9C, employing the inevitably different but most suitable experimental designs depending on the different kinetic properties, we were able to compare the rates of the E2P to E1PCa₂ reverse transition induced by the luminal Ca²⁺ binding to the transport sites of E2P at the limited Ca²⁺ concentration range up to 3 mM. In the wild type in the presence of K⁺, the rate was Ca²⁺-dependent and not saturated even at 3 mM, thus reflecting at least the Ca²⁺-dependent and rate-limiting process; *i.e.* the luminal Ca²⁺-induced change from E2P to E2PCa₂. This reverse transition rate in the wild type in the presence of K⁺ was significantly faster than those in the wild type in the absence of K⁺ and in Y122A (as well as in the other Y122-HC mutants (supplemental Fig. S3)) especially at the high Ca²⁺ concentration over 1 mM.

Here it is also interesting to note that the affinity of E2P for the luminal Ca²⁺ in the wild type without K⁺ and the Y122-HC mutants is significantly higher than in the wild type with K⁺ (see Fig. 8B). If the rate of luminal Ca²⁺ access and binding to E2P is solely slowed in the wild type without K⁺ and Y122-HC mutants, a decrease in the affinity is rather the consequence, which is in contrast to the observed increase. Therefore the rates of the Ca²⁺ release from E2PCa₂ in the wild type without K⁺ and in the Y122-HC mutants are also presumably retarded significantly as compared with that in the wild type in the presence of K⁺. Namely, the mutations of Y122-HC and the lack of K⁺ binding affect the energy levels of Ca²⁺-free and -bound E2P states, as well as that of the transition state for luminal gating (opening), and favor the Ca²⁺-bound state E2PCa₂ and the closed luminal gate.

DISCUSSION

Roles of Y122-HC in Ca²⁺ Release from E2PCa₂ and in E2P Hydrolysis—In this study, we found that the mutations of any of the seven residues in Y122-HC increase the luminal Ca²⁺ affinity and retard the luminal Ca²⁺ access to the transport sites in E2P. These mutations also retard markedly the hydrolysis of the Ca²⁺-released form of E2P (22, 23). Thus, the proper formation of Y122-HC from the seven residues is critical for both Ca²⁺ release

Tyr¹²²-hydrophobic Cluster of SERCA1a for Ca²⁺ Release

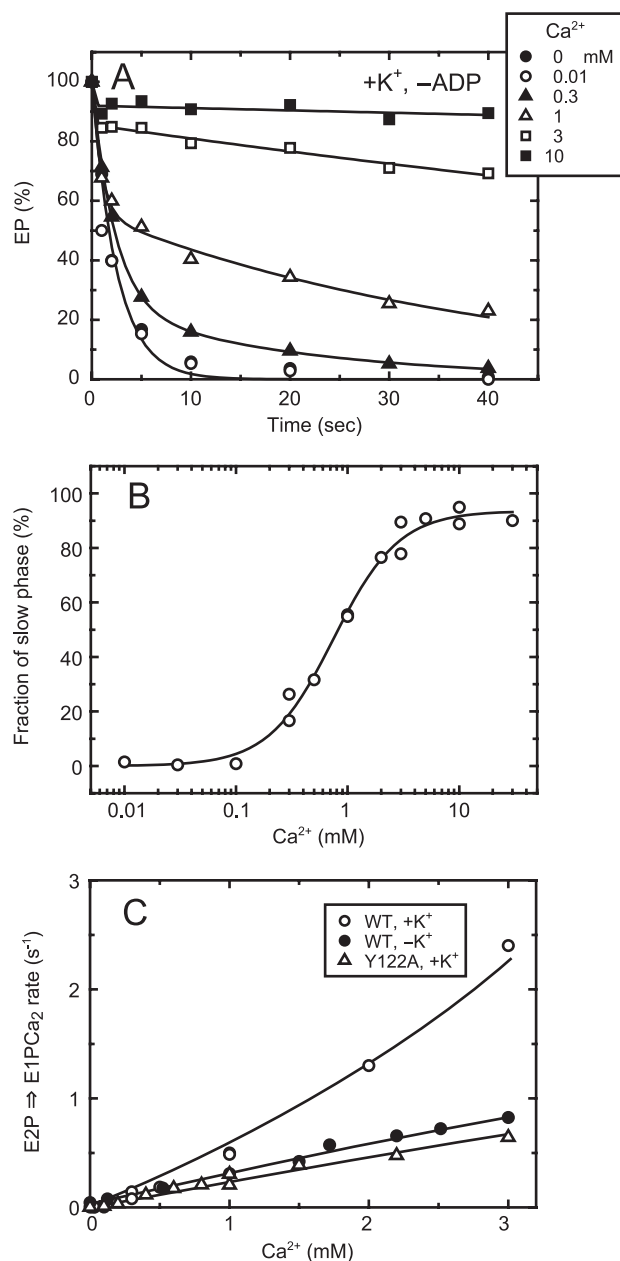


FIGURE 9. Kinetics of luminal Ca²⁺-induced change of E2P to E1PCa₂ in the wild type in the presence of K⁺ without ADP. *A*, the microsomes expressing the wild type were phosphorylated with ³²P_i in the presence of A23187 and absence of Ca²⁺ and chilled on ice, as described in Fig. 7. Subsequently, the phosphorylated sample was mixed at 0 °C with a 20-fold volume of chase solution containing 105 mM KCl and various concentrations of CaCl₂ without ADP, otherwise as described in Fig. 7. The final free Ca²⁺ concentrations were indicated in the figure. At the indicated time periods after this addition, the chase reaction was terminated by trichloroacetic acid, and the amount of EP was determined. *Solid lines* show the least squares fit to a double exponential decay. The EP remaining in the second and slow phase was all in the ADP-sensitive form (thus E1PCa₂, data not shown), and the first and rapid phase is the forward hydrolysis of E2P without bound Ca²⁺. *B*, the fraction of EP in the second phase in the total amount of EP was obtained by extrapolating to the zero time in the double exponential decay fitting, and plotted *versus* the Ca²⁺ concentration. The data were fitted well with the Hill equation (*solid line*), and the Ca²⁺ concentration giving the 50% saturation and the Hill coefficient were found to be 750 μM and 1.5. Here note that the EP amount in the second phase is dependent on the ratio between the rate of the forward E2P hydrolysis and that of the reverse E2P to E1PCa₂ conversion upon the luminal Ca²⁺ binding to E2P: the plot reflects the relative values between these forward and reverse rates of E2P rather than the luminal Ca²⁺ affinity of E2P. *C*, by using the data obtained in *A* and *B* with the wild type in the presence of K⁺, the rate of the luminal Ca²⁺-induced E1PCa₂ formation

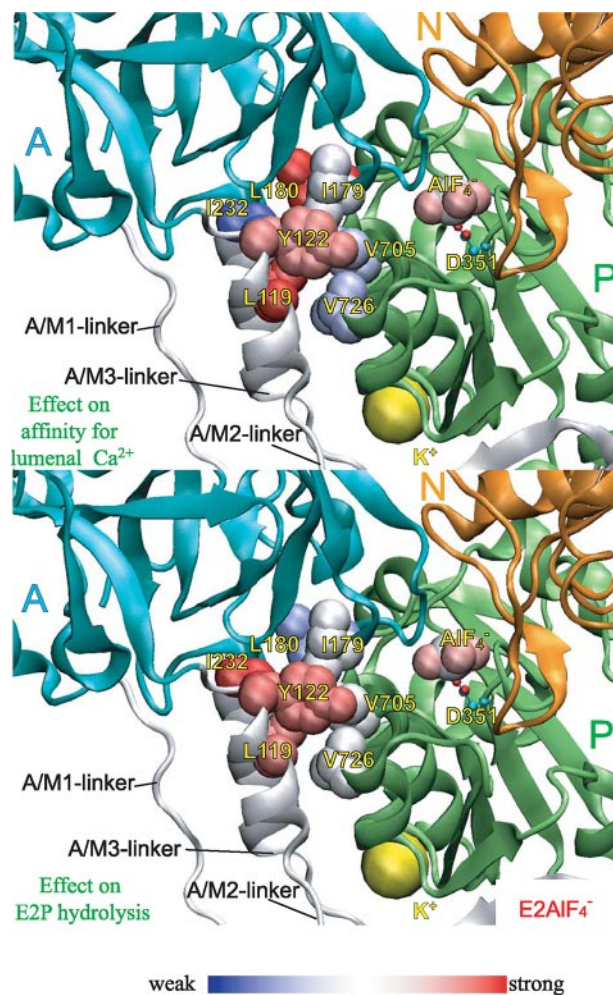


FIGURE 10. Strength of the mutational effects of seven residues in Tyr¹²²-hydrophobic cluster on E2P hydrolysis and luminal Ca²⁺ affinity. The detailed structure at Y122-HC is shown with E2-ALF₄ (the analog for E2~P, the transition state of the E2P hydrolysis (21), PDB code: 1XP5 (15)). The seven residues involved in Y122-HC (Tyr¹²²/Leu¹¹⁹, Ile¹⁷⁹/Leu¹⁸⁰, Ile²³², and Val⁷⁰⁵/Val⁷²⁶), ALF₄ bound at the phosphorylation site Asp³⁵¹, and the bound potassium ion are shown by van der Waals spheres. The seven residues in Y122-HC are colored differently based on the strength of the retardation of the E2P hydrolysis rate (*lower panel*) and that of the increase in the luminal Ca²⁺ affinity (*upper panel*). The color changes gradually from red for the strongest effects to blue for weakening.

into lumen from E2PCa₂ (reducing the Ca²⁺ affinity and opening the luminal gate), and formation of the E2P catalytic site for the subsequent Asp³⁵¹-acylphosphate hydrolysis. The formation of Y122-HC therefore functions critically for realizing and stabilizing the compactly organized and thus distorted structure of the Ca²⁺-released form of E2P. The stabilization of this state is certainly important for making the time period long enough for Ca²⁺ release into lumen and likely for proton bindings to the empty Ca²⁺ sites, and for the fine rearrangement of the catalytic site for the subsequent Asp³⁵¹-acylphosphate hydrolysis.

As shown in Fig. 10 and supplemental Fig. S4, the extents of the mutational effects on the luminal Ca²⁺ affinities and on the

from E2P (k_{rev} (○)) was calculated at each Ca²⁺ concentration by the equation, $k_{rev} = k_i F_s / (1 - F_s)$. Here, F_s is the fraction of EP in the second phase, and k_i is the forward hydrolysis rate of E2P without Ca²⁺. For comparison with the wild type in the absence of K⁺ (●) and Y122A in the presence of K⁺ (△), their luminal Ca²⁺ access rates (the rates of the luminal Ca²⁺-induced reverse E2P decay via E1PCa₂ in the presence of ADP) obtained in Fig. 8A are plotted.

E2P hydrolysis rates varied significantly among the seven Y122-HC mutants and depended on their positions. The residues of which mutation exhibited the strongest effects on increasing luminal Ca²⁺ affinity were Leu¹¹⁹, Tyr¹²², and Leu¹⁸⁰. This agrees with the critical role of M2 for rearrangement of the transmembrane helices for the Ca²⁺ release; *i.e.* the tight association of the top part of M2 with the largely rotating A domain in Y122-HC functions for the lever-like inclination of M2 to push the luminal part of M4 to open the luminal gate (14). In fact, in *E2PCa*₂, trapped by the elongation of the A/M1-linker, the Leu¹¹⁹/Tyr¹²² region on the top part of M2 is not involved fully in Y122-HC (9).

The residues of which mutations exhibited the strongest retardation of the *E2P* hydrolysis were Ile²³² at the top part of the A/M3-linker and, again, Leu¹¹⁹ and Tyr¹²² on the A/M2-linker (top part of M2). Thus these residues on the linkers seem to contribute most critically to produce the proper configuration of the catalytic site. Consistently, the proteolytic cleavage at Leu¹¹⁹ on the A/M2-linker causes a marked inhibition of the *E2P* hydrolysis (43). The structural changes producing the Ca²⁺ release may be transmitted to the catalytic site via these residues of Y122-HC on the linkers, thereby ensuring the *E2P* hydrolysis to occur after the Ca²⁺ release. In any case, the different degree of the contributions of the seven residues of Y122-HC to the Ca²⁺ release and subsequent formation of the *E2P* catalytic site may suggest a possible sequential gathering of the seven residues. This possibility will be discussed more in the last section of "Discussion" in relation to the crystal structure *E2*·BeF₃⁻ (17, 18).

Structural Mechanism Involving Y122-HC and Other Critical Elements—In *E1Ca*₂·AlF₄⁻·ADP → *E2*·MgF₄²⁻ as an overall structural change, including the *EP* isomerization and Ca²⁺ release (supplemental Fig. S5A), the A domain largely rotates and M2 largely inclines. Also the P domain markedly inclines toward the lower side of the A domain and rotates by ~20° around the phosphorylation site (Asp³⁵¹) parallel to the membrane and in the opposite direction of the A-domain rotation. These motions involve (can be dissected into) the horizontal and vertical factors, parallel and perpendicular to the membrane plane. As a consequence of the motions, the A and P domains and M2 will come to their appropriate positions producing their tight association at Y122-HC. At the A-P domain interface in the *E2P* analog structures, there is another interaction network between these domains at the Val²⁰⁰ loop, Asp¹⁹⁶–Asp²⁰³ of the A domain (Fig. 1, and see supplemental Fig. S3 in Ref. 23 for the details of the interactions and central role of Val²⁰⁰). Our previous mutations of Val²⁰⁰ showed (24) that this A-P domain interaction is critical for Ca²⁺ release from *E2PCa*₂ and for formation of the *E2P* catalytic site, thus very similarly to Y122-HC. Then note that, in the *E2P* analog structures (see supplemental Fig. S5A for *E2*·MgF₄²⁻), the two networks at Y122-HC and at Val²⁰⁰ are located at each side of the A-P domain interface on its *top view* and at the bottom and upper parts of the interface, respectively on its *side view*. Thus the two are situated horizontally and vertically with the specific relative positioning. It is very likely that this positioning of the two is most efficiently functioning to realize and stabilize the compactly organized and distorted structure of the Ca²⁺-re-

leased *E2P*: *i.e.* the interactions at the two positions are most appropriate to produce the horizontal and vertical motions of the P and A domains and M2 required for Ca²⁺ release from *E2PCa*₂ and to stabilize the Ca²⁺-released *E2P* state. Certainly these motions cause the rearrangements in the transmembrane helices for Ca²⁺ release: *e.g.* the P-domain inclination with slight rotation is directly associated with the bending and slight rotation of connected M4/M5 and downward movement of M4, thus their twisting-like motion. The largely inclining M2 pushes the luminal part of M4 (supplemental Fig. S5B). Hence the Ca²⁺ sites are destroyed, and the luminal gate is opened.

It should be noted that, for the loss of the ADP sensitivity *E1PCa*₂ → *E2PCa*₂, the large rotation of the A domain and its docking onto the P domain should occur so as to bring the T¹⁸¹GES loop above Asp³⁵¹-acylphosphate to block the ADP access from the N domain. As the motive force of this large A-domain rotation approximately parallel to membrane plane, the strain imposed on the A/M3-linker in *E1PCa*₂ was predicted to be critical (13, 14, 20, 44). Also, the sufficiently long length of the A/M1-linker was revealed to be critical for this *EP* isomerization, in this case, probably for realizing the *E2PCa*₂ structure, in which the A domain is positioned above the P domain (9, 45). For the subsequent Ca²⁺ release in *E2PCa*₂ → *E2P* + 2Ca²⁺, the A/M1-linker with its appropriately short length (therefore its strain) is critical (9). Actually, the elongation of this linker blocks completely Ca²⁺ deocclusion/release from *E2PCa*₂, thus trapping this *E2PCa*₂ state in which Y122-HC is not properly formed yet in contrast to its proper formation in the Ca²⁺-released form of *E2P* with the lumenally opened normal Ca²⁺ release pathway (9). The results clearly demonstrated that the native and appropriately short length of A/M1-linker functions critically in inducing the motions from the *E2PCa*₂ state, especially inclination of the A and P domains and M2, to accomplish the Y122-HC formation and the Ca²⁺ deocclusion/release from *E2PCa*₂. During the Y122-HC formation, the interaction force being produced in Y122-HC will likely function to induce the final process of the vertical and horizontal motions of the P and A domain and M2 to realize and stabilize the Ca²⁺-released *E2P* structure (supplemental Fig. S6). Importantly also, the *E2P* catalytic site is produced by these rearrangements. In this mechanism, a possible hydrolysis of Asp³⁵¹-acylphosphate without releasing Ca²⁺ will be avoided; thereby the ordered reaction sequence of the Ca²⁺ release from *E2PCa*₂ and the subsequent *E2P* hydrolysis will be accomplished for the energy coupling.

Possible Structural Role of K⁺ for Reducing Ca²⁺ Affinity and Luminal Gating—K⁺ is known to markedly accelerate the *E2P* hydrolysis (35, 36) and also to modulate the *E2* to *E1Ca*₂ transition in the non-phosphorylated Ca²⁺-ATPase (46, 47). In the present study, we further found that the K⁺ binding is important for reducing the affinity for Ca²⁺ and luminal gating thus for Ca²⁺ release from *E2PCa*₂. In the crystal structure *E1Ca*₂·AlF₄⁻·ADP, K⁺ is situated at the bottom part of the P domain and coordinated by the backbone carbonyls of the loop Leu⁷¹¹–Glu⁷¹⁵ and by the Glu⁷³² side chain (Fig. 11). The K⁺ binding at this site was indeed previously found by the mutations to be critical for the stimulation of the *E2P* hydrolysis (37). In the structures *E2P* analogs and *E2(TG)*, this K⁺ site of the P

Tyr¹²²-hydrophobic Cluster of SERCA1a for Ca²⁺ Release

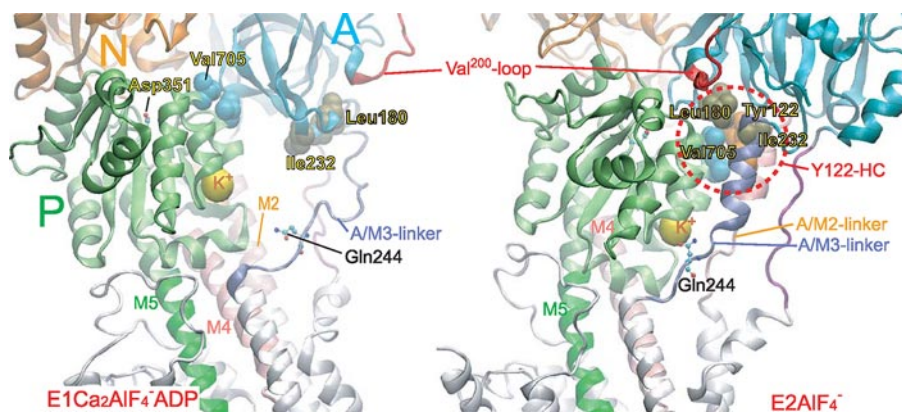


FIGURE 11. Bound K⁺ and Tyr¹²²-hydrophobic cluster in crystal structures. The part of structures *E1Ca₂·AlF₄·ADP* (*E1~PCa₂·ADP* analog, *left*) and *E2·AlF₄⁻* (*E2~P* analog, *right*) around Y122-HC and the bound K⁺ ion are shown in schematic models (PDB codes: 1T5T and 1XP5 (12, 15)). The two structures were manually aligned with M8–M10 helices, which do not move virtually in the two. K⁺ bound in these structures is shown by a yellow van der Waals sphere. Gln²⁴⁴ on the A/M3-linker at the immediate vicinity of the bound K⁺ in *E2·AlF₄⁻* is indicated by ball and stick model.

domain comes very close to the A/M3-linker, and actually K⁺ at this site is further coordinated by the Gln²⁴⁴ side chain on the A/M3-linker (see *E2·AlF₄⁻* in Fig. 11). Because the alanine substitution of Gln²⁴⁴ and those of Glu-Gln-Asp²⁴⁵ gave virtually no effect on Ca²⁺ transport activity (48), K⁺ at this region may be coordinated by their neighboring residues or backbone carbonyls on the A/M3-linker and thereby perform a structural function. In the present study, we found that the lack of K⁺ binding has the consequences very similar to those of the mutations at Y122-HC. It is therefore possible that the K⁺ binding functions with similar structural effects as Y122-HC to produce the proper structure of the Ca²⁺-released form of *E2P*.

Then note that the K⁺ site of the P domain in *E1Ca₂·AlF₄·ADP* is situated at much higher position from the membrane plane than the Gln²⁴⁴ region on the A/M3-linker (Fig. 11) and that, in the change *E1Ca₂·AlF₄·ADP* → *E2·AlF₄⁻* (or *E2·BeF₃⁻* and *E2·MgF₄²⁻*), the P domain with connected M4/M5 largely inclines toward the A domain, hence the K⁺ site with bound K⁺ on the P domain moves down to the Gln²⁴⁴ region on the A/M3-linker to make contact. The interactions between the bottom part of the P domain and the A/M3-linker via bound K⁺ thus produced would likely cross-link them and hence contribute to formation and stabilization of this compactly organized Ca²⁺-released structure of *E2P* with the reduced Ca²⁺ affinity and lumenally opened gate. Alternatively, it is also possible that the appropriate P-domain structure produced by K⁺ binding on this domain solely contributes to the formation of the Ca²⁺-released *E2P* structure.

Y122-HC in Crystal Structure of *E2·BeF₃⁻*—The crystal structures of *E2·BeF₃⁻*, the analog for the *E2P* ground state (21), were solved at the atomic level very recently with and without bound thapsigargin, TG (*E2BeF₃⁻* and *E2BeF₃⁻* (TG) (17, 18)). Surprisingly, in this crystallized *E2·BeF₃⁻*, the side chains of Ile¹¹⁹ and Tyr¹²² are somewhat pointing away from the clustered other five residues on the A and P domains (Ile¹⁷⁹/Leu¹⁸⁰/Ile²³² and Val⁷⁰⁵/Val⁷²⁶), although all these seven residues are closely located in the *E2·BeF₃⁻* structures of both 2ZBE (17) and 3B9B (18). On the other hand, Y122-HC is formed fully from all these seven residues in *E2BeF₃⁻* (TG) as well as in the other *E2P* anal-

ogous structures, *E2·AlF₄⁻* and *E2·MgF₄²⁻*. Thus, the assembling manner of the seven residues in the crystal structure *E2·BeF₃⁻* seemingly conflicts with our results that the gathering of all the seven residues, including Tyr¹²²/Ile¹¹⁹ in Y122-HC, is required for producing the Ca²⁺-released *E2P*. Furthermore, Tyr¹²² and Ile¹¹⁹ on the top part of M2 (A/M2-linker) are likely most critical in Y122-HC and play central roles (Fig. 10). Our previous biochemical structural analysis of SR Ca²⁺-ATPase in solution by the proteolysis and the luminal Ca²⁺ accessibility demonstrated (21) that, in *E2·BeF₃⁻* without TG, Leu¹¹⁹/Tyr¹²² are surely gathered

and involved in Y122-HC, and thereby the luminal gate is opened and the luminal Ca²⁺ is accessible to the transport sites. Thus the crystal structure *E2·BeF₃⁻* seems to conflict also with these biochemical results obtained in solution.

Nevertheless, as a comprehensive idea, the crystal structure of *E2·BeF₃⁻* may be consistent with (or indicative of) the view that the gathering of the seven residues to form Y122-HC upon motions of the A and P domains and M2 (A/M2-linker) occurs in some ordered sequence but not necessarily at once (see Fig. 10 and under “Discussion”). Most peculiar to us is that Tyr¹²² and Leu¹¹⁹, of which mutations exhibited the most inhibitory effects, are not involved yet in the hydrophobic cluster in the crystal structure *E2·BeF₃⁻*. Here note that, in the structure *E2·BeF₃⁻*, a Mg²⁺ ion is bound near the Ca²⁺ binding sites in the transmembrane domain because an extremely high Mg²⁺ concentration employed for crystallization (18), or protonation on the residues of transmembrane helices, including Ca²⁺ ligands, must have occurred as in low pH for crystallization (17). Thus, these ligations are probably involved critically in the stabilization of the transmembrane helices for the crystallization. This might mean that the transmembrane structure thus stabilized differs from that without any ligations, *i.e.* the state immediate after the Ca²⁺ release (the empty Ca²⁺ sites) that is realized by the contribution of Y122-HC. Therefore, Y122-HC is, in return, disrupted or not properly produced yet in the crystal structure *E2·BeF₃⁻* as if it occurs with the luminal Ca²⁺ binding in the *E2PCa₂* state as postulated in this study. Therefore the following sequential gathering of the seven residues to produce Y122-HC can be speculated: The five hydrophobic residues on the A domain (Ile¹⁷⁹/Leu¹⁸⁰/Ile²³²) and P domain (Val⁷⁰⁵/Val⁷²⁶) are first gathered through the motions of the A and P domains and top part of M2 (A/M2-linker), and subsequently, the top part of M2, including Ile¹¹⁹ and Tyr¹²², makes further motions during the final process of the M2 inclination to join them and produce the fully assembled Y122-HC, thereby to realize and stabilize fully the gathered state of the A and P domains and top part of M2 (A/M2-linker) as in the Ca²⁺-released form of *E2P*. Being in agreement with this view, in *E2PCa₂* trapped by the elongation of the A/M1-linker, Leu¹¹⁹/

Tyr¹²² on the top part of M2 is not fully involved yet in Y122-HC (9). The Ca²⁺-released and empty Ca²⁺ sites (without any protonation and stabilization immediately after the Ca²⁺ release) will be subsequently protonated producing the E2P ground state for its hydrolysis.

Alternatively, if a possible contribution of such ligation in the transmembrane domain (Mg²⁺ or protonation) should not be concerned in the crystallization of E2·BeF₃⁻, the followings might be possible: first of all, the arrangements of helices of the Ca²⁺-released empty transport sites must be unstable, for example, due to possible repulsions between the negative charges of the Ca²⁺ ligands. Then to relieve the instability, the most effective gathering of Tyr¹²²/Leu¹¹⁹ in Y122-HC, which produces and stabilizes the Ca²⁺-released empty state, might possibly be disrupted; thereby the helices may be rearranged so as to form the more stabilized arrangements that can be crystallized.

Acknowledgments—We thank Dr. David H. MacLennan, University of Toronto, for his generous gift of SERCA1a cDNA and Dr. Randal J. Kaufman, Genetics Institute, Cambridge, MA, for his generous gift of the expression vector pMT2. We are also grateful to Dr. Chikashi Toyoshima, University of Tokyo, for helpful discussions.

REFERENCES

- Hasselbach, W., and Makinose, M. (1961) *Biochem. Z.* **333**, 518–528
- Ebashi, S., and Lipmann, F. (1962) *J. Cell Biol.* **14**, 389–400
- Inesi, G., Sumbilla, C., and Kirtley, M. E. (1990) *Physiol. Rev.* **70**, 749–776
- Møller, J. V., Juul, B., and le Maire, M. (1996) *Biochim. Biophys. Acta* **1286**, 1–51
- MacLennan, D. H., Rice, W. J., and Green, N. M. (1997) *J. Biol. Chem.* **272**, 28815–28818
- McIntosh, D. B. (1998) *Adv. Mol. Cell. Biol.* **23A**, 33–99
- Toyoshima, C., and Inesi, G. (2004) *Annu. Rev. Biochem.* **73**, 268–292
- Toyoshima, C. (2008) *Arch. Biochem. Biophys.* **476**, 3–11
- Daiho, T., Yamasaki, K., Danko, S., and Suzuki, H. (2007) *J. Biol. Chem.* **282**, 34429–34447
- Toyoshima, C., Nakasako, M., Nomura, H., and Ogawa, H. (2000) *Nature* **405**, 647–655
- Toyoshima, C., and Nomura, H. (2002) *Nature* **418**, 605–611
- Sørensen, T. L.-M., Møller, J. V., and Nissen, P. (2004) *Science* **304**, 1672–1675
- Toyoshima, C., and Mizutani, T. (2004) *Nature* **430**, 529–535
- Toyoshima, C., Nomura, H., and Tsuda, T. (2004) *Nature* **432**, 361–368
- Olesen, C., Sørensen, T. L.-M., Nielsen, R. C., Møller, J. V., and Nissen, P. (2004) *Science* **306**, 2251–2255
- Takahashi, M., Kondou, Y., and Toyoshima, C. (2007) *Proc. Natl. Acad. Sci. U. S. A.* **104**, 5800–5805
- Toyoshima, C., Norimatsu, Y., Iwasawa, S., Tsuda, T., and Ogawa, H. (2007) *Proc. Natl. Acad. Sci. U. S. A.* **104**, 19831–19836
- Olesen, C., Picard, M., Winther, A.-M. L., Gyrupe, C., Morth, J. P., Oxvig, C., Møller, J. V., and Nissen, P. (2007) *Nature* **450**, 1036–1042
- Danko, S., Daiho, T., Yamasaki, K., Kamidochi, M., Suzuki, H., and Toyoshima, C. (2001) *FEBS Lett.* **489**, 277–282
- Danko, S., Yamasaki, K., Daiho, T., Suzuki, H., and Toyoshima, C. (2001) *FEBS Lett.* **505**, 129–135
- Danko, S., Yamasaki, K., Daiho, T., and Suzuki, H. (2004) *J. Biol. Chem.* **279**, 14991–14998
- Yamasaki, K., Daiho, T., Danko, S., and Suzuki, H. (2004) *J. Biol. Chem.* **279**, 2202–2210
- Wang, G., Yamasaki, K., Daiho, T., and Suzuki, H. (2005) *J. Biol. Chem.* **280**, 26508–26516
- Kato, S., Kamidochi, M., Daiho, T., Yamasaki, K., Wang, G., and Suzuki, H. (2003) *J. Biol. Chem.* **278**, 9624–9629
- Kaufman, R. J., Davies, M. V., Pathak, V. K., and Hershey, J. W. B. (1989) *Mol. Cell. Biol.* **9**, 946–958
- Maruyama, K., and MacLennan, D. H. (1988) *Proc. Natl. Acad. Sci. U. S. A.* **85**, 3314–3318
- Kanazawa, T., Saito, M., and Tomomura, Y. (1970) *J. Biochem. (Tokyo)* **67**, 693–711
- Weber, K., and Osborn, M. (1969) *J. Biol. Chem.* **244**, 4406–4412
- Daiho, T., Suzuki, H., Yamasaki, K., Saino, T., and Kanazawa, T. (1999) *FEBS Lett.* **444**, 54–58
- Lowry, O. H., Rosebrough, N. J., Farr, A. L., and Randall, R. J. (1951) *J. Biol. Chem.* **193**, 265–275
- Humphrey, W., Dalke, A., and Schulten, K. (1996) *J. Mol. Graphics* **14**, 33–38
- Coan, C., Verjovski-Almeida, S., and Inesi, G. (1979) *J. Biol. Chem.* **254**, 2968–2974
- Prager, R., Punzengruber, C., Kolassa, N., Winkler, F., and Suko, J. (1979) *Eur. J. Biochem.* **97**, 239–250
- de Meis, L., and Inesi, G. (1982) *J. Biol. Chem.* **257**, 1289–1294
- Shigekawa, M., and Pearl, L. J. (1976) *J. Biol. Chem.* **251**, 6947–6952
- Shigekawa, M., and Dougherty, J. P. (1978) *J. Biol. Chem.* **253**, 1451–1457
- Sørensen, T. L.-M., Clausen, J. D., Jensen, A.-M. L., Vilsen, V., Møller, J. V., Andersen, J. P., and Nissen, P. (2004) *J. Biol. Chem.* **279**, 46355–46358
- de Meis, L., Martins, O. B., and Alves, E. W. (1980) *Biochemistry* **19**, 4252–4261
- Fersht, A. R. (1999) *Structure and Mechanism in Protein Science: A Guide to Enzyme Catalysis and Protein Folding*, pp. 132–168, W. H. Freeman and Co., New York
- Sato, K., Yamasaki, K., Daiho, T., Miyauchi, Y., Takahashi, H., Ishida-Yamamoto, A., Nakamura, S., Iizuka, H., and Suzuki, H. (2004) *J. Biol. Chem.* **279**, 35595–35603
- Shigekawa, M., Wakabayashi, S., and Nakamura, H. (1983) *J. Biol. Chem.* **258**, 8698–8707
- Wakabayashi, S., and Shigekawa, M. (1987) *J. Biol. Chem.* **262**, 11524–11531
- Lenoir, G., Picard, M., Gauron, C., Montigny, C., Le Maréchal, P., Falson, P., le Maire, M., Møller, J. V., and Champeil, P. (2004) *J. Biol. Chem.* **279**, 9156–9166
- Møller, J. V., Lenoir, G., Marchand, C., Montigny, C., le Maire, M., Toyoshima, C., Juul, B. S., and Champeil, P. (2002) *J. Biol. Chem.* **277**, 38647–38659
- Daiho, T., Yamasaki, K., Wang, G., Danko, S., and Suzuki, H. (2003) *J. Biol. Chem.* **278**, 39197–39204
- Lee, A. G., Baker, K., Khan, Y. M., and East, J. M. (1995) *Biochem. J.* **305**, 225–231
- Champeil, P., Henao, F., and de Foresta, B. (1997) *Biochemistry* **36**, 12383–12393
- Clarke, D. M., Maruyama, K., Loo, T. W., Leberer, E., Inesi, G., and MacLennan, D. H. (1989) *J. Biol. Chem.* **264**, 11246–11251